JOURNAL OF CATALYSIS 157, 687–697 (1995)

The Role of Fe and Co Dopants during the Activation of the $VO(HPO_4) \cdot 0.5H_2O$ Precursor of the Vanadium Phosphorus Catalyst as Studied by *in Situ* Laser Raman Spectroscopy

I. Study of $VO(HPO_4) \cdot 0.5H_2O$ Precursors Prepared by Reduction of V_2O_5 by Isobutanol

F. Ben Abdelouahab,*,†,‡ R. Olier,†,[1] M. Ziyad,‡ and J. C. Volta*

*Institut de Recherches sur la Catalyse, CNRS, 2 Avenue A. Einstein, 69626, Villeurbanne, Cédex, France; †Laboratoire de Physicochimie des Interfaces, Ecole Centrale de Lyon, 36 Avenue Guy de Collongue, BP 163, 69131, Ecully Cédex, France; and ‡Laboratoire de Catalyse et Matériaux, Université de Rabat, Av. Ibn Batouta, Rabat, Maroc

Received April 19, 1995; revised August 24, 1995

The activation of two Fe- and Co-doped $VO(HPO_4) \cdot 0.5H_2O$ precursors under *n*-butane/air catalytic atmosphere (1.5%) has been compared to the corresponding undoped precursor prepared under the same conditions by the organic route of reduction of V_2O_5 by isobutanol. The modification of the structure of the VPO materials has been followed by *in situ* laser Raman spectroscopy during the activation on line. It is evidenced that doping promotes the first time the oxidation of the catalysts favoring the $VOPO_4/(VO)_2P_2O_7$ balance. This is confirmed by an analysis of the bulk and surface composition of the final catalysts by UV-visible, XPS spectroscopy and ^{31}P NMR by spin-echo mapping. The role of the two dopants is shown to be different on the catalytic performances: both Co and Fe dopants improve strongly selectivity to maleic anhydride but *n*-butane conversion is decreased for Co and increased for Fe. This has been explained by a different dispersion of $VOPO_4$ phases on the $(VO)_2P_2O_7$ matrix during the activation process as compared to the same undoped VPO catalyst.

INTRODUCTION

All catalysts used industrially for the production of maleic anhydride from *n*-butane are based on vanadium–phosphorus oxides (1–5).

It is considered that the improvement of the catalytic performances of the VPO system goes through a better knowledge of "some key structural and surface aspects of the catalyst that characterize its specific ability in the selective transformation of butane" (5). One of the main questions to answer is "What is the real nature of the active surface of vanadyl pyrophosphate during catalytic reaction?" (5) and What is going on during the activation procedure of the VPO precursor and particularly from the period of short time of activation on stream (100 h) to longer periods (1000 h) which correspond to "equilibrated catalysts" along which catalytic performances improve? As a consequence, direct information, in the course of the catalytic reaction, on the transformation of the precursor to the final catalyst is crucial to approaching, on line, the structural characteristics of the VPO catalyst at a short range order scale.

It is generally accepted that the monophasic vanadyl pyrophosphate is the active phase in *n*-butane oxidation, but there are no clear and univocal data that demonstrate this belief (2). For the valence state of vanadium in the active surface, an equilibrium V^{4+}/V^{5+} on the surface of vanadyl pyrophosphate during *n*-butane oxidation has been demonstrated and was shown to depend on time of activation (4, 6, 7).

The selectivity to maleic anhydride was proposed to be connected to the presence of a very limited and controlled amount of V^{5+} sites on the $(VO)_2P_2O_7$ matrix (4). It has been recently demonstrated by Raman spectroscopy using an *in situ* cell that the transformation of the $VO(HPO_4)$, $0.5\ H_2O$ precursor under the *n*-butane/air catalytic atmosphere (1.5%) goes through a complete amorphization of the structure of the VPO material which precludes a reoxidation to the $VOPO_4$ phases (δ, α_{II}, perhaps γ), a further interconversion of these $VOPO_4$ phases (δ to α_{II}) and a final reduction of the $VOPO_4$ phases to sublying

[1] Present address: Department de Chimie, Faculté des Sciences, Avenue Le Gorgeu, 29200, Brest, France.

0021-9517/95 $12.00

$(VO)_2P_2O_7$, which simultaneously improves its crystallinity (8).

During the activation period, the analysis of the composition of the bulk and the surface of the catalysts has been performed by XPS, ^{31}P MAS–NMR, and ^{31}P NMR by spin-echo mapping. It was evidenced that the initial reoxidation to $VOPO_4$ proceeded at the surface of the catalyst grains (9). As the time of activation increases and when the $VOPO_4$ phases are reduced, there is a progressive dissolution of V^{5+} ions into the bulk of the $(VO)_2P_2O_7$ matrix as evidenced by the increase of the electron conductivity (10).

The examination of the patent literature on the VPO system for *n*-butane oxidation to maleic anhydride shows that the catalytic performance can be improved by doping the materials with suitable elements. Several reviews and publications have been devoted to this question (3, 11–14). From the published results, it appears that the role of the promoter is far from clear. Some authors found that a number of cations (Co, Fe, Li, Zn, Ce, Mn, Sn, and Lu) formed solid solutions in $(VO)_2P_2O_7$ (11, 15–17). It was proposed that this ensures that the active catalyst compound contains the excess phosphorus required to maintain its stability in an oxidizing environment (3). From XPS data, it was shown that the addition of cobalt ions to VPO catalysts increased the phosphorous content at the surface (increase in P/V ratio) (13). It was concluded that this should have the effect of prolonging the catalyst lifetime (13). This is in agreement with the fact it is necessary to add some phosphorous compound on line in the *n*-butane/air reacting atmosphere to maintain a longer life for the industrial catalysts (4). It has also been shown that the exposure of the catalyst to the hydrocarbon–air mixture tends to result in reduction of the catalyst (5, 9, 18). As a consequence, it can be hypothesized that the promoter should influence the V^{4+}/V^{5+} surface distribution and thus influence the conditions of reaching the stationary state and influence the final catalytic performance.

Very few systematic studies have been reported on the effect of the promoter on the VPO catalytic system. In this publication, and in the continuity of our previous study on the transformation of the $VOHPO_4$, 0.5 H_2O precursor as followed by *in situ* Raman spectroscopy (8), we examine the modifications induced on the physicochemistry of the VPO system doped by the two promoters Fe and Co at low level (M/V = 5%) during the period of its activation under the *n*-butane/air reacting atmosphere, in comparison with an undoped VPO material. This first contribution concerns a doped $VOHPO_4$, 0.5 H_2O precursor prepared according to the organic Exxon route with isobutanol as reducing reagent (19). A second contribution concerns a doped $VOHPO_4 \cdot 0.5H_2O$ precursor with a different morphology prepared by reduction of $VOPO_4 \cdot 2H_2O$ by isobutanol (20, 21).

EXPERIMENTAL

Preparation of the Undoped and Doped $VOHPO_4$, 0.5 H_2O Precursors

Undoped precursor $VOHPO_4 \cdot 0.5H_2O$ was prepared by adding V_2O_5 (11.8 g) to isobutanol (250 ml). H_3PO_4 (16.49 g 85%) was then introduced to the mixture, which was then refluxed for 16 h. The light blue suspension was then separated from the organic solution by filtration and washed with isobutanol (200 ml) and ethanol (150 ml, 100%). The resulting solid was refluxed in water (9 ml H_2O/g solid), filtered hot, and dried in air (110°C, 16 h). For the preparation of the two doped 5% Fe and Co/V precursors, the required mass of the corresponding acetylacetonate salts was previously dissolved in isobutanol according to the atomic M/V stoichiometry, prior to refluxing with isobutanol and 85% H_3PO_4. Further operations of filtration and washing were identical to the undoped precursor. The three precursors were then dried at 120°C under air for 12 h.

Precursors and Catalysts Characterization

A schematic diagram of the *in situ* cell, constructed at the Institut de Recherches sur la Catalyse and used at Ecole Centrale de Lyon for the laser Raman study of the VPO materials, has been previously presented (8–22). It is shown in Fig. 1. It was made of three parts of stainless steel with different functions. The VPO precursor to be examined under reaction conditions was introduced in the lower part on a glass sintered disc. Material, 1.5 g, corresponding to an approximate volume of 2 cm^{-3} was generally used for each study. The temperature was controlled by a thermocouple in the center of the catalyst powder. The reaction gases flew through the powder in the middle of this lower part which was heated by three thermoregulated fingers. The upper part held a glass window transparent to the laser beam. The gaseous effluent from the cell was analyzed by gas chromatography. The tightness of the cell was ensured by two gold wires. The composition and flow rate of the reacting gases (1.5% butane/air) were controlled by two flow meters. Experiments were done with a GSHV of 2000 h^{-1}. Detection of evolved gases was done by a FID detector from DELSI. CO and CO_2 were quantitatively transformed to CH_4 on a Ni Raney catalyst working at 300°C. It was thus possible to analyze all the gases with the only FID detector. Two columns were used in parallel: a 1-m × 1/4-in. Porapak Q column to separate CO and CO_2 which were further transformed into CH_4, when butane, acetic, acrylic acids and maleic anhydride were separated on a 3-m × 1/8-in. Lac 2R (13%)/H_3PO_4 (2.5%) on Gas Chrom Q column. The two columns were heated at 140°C. The tube connecting the cell to the chromatograph was

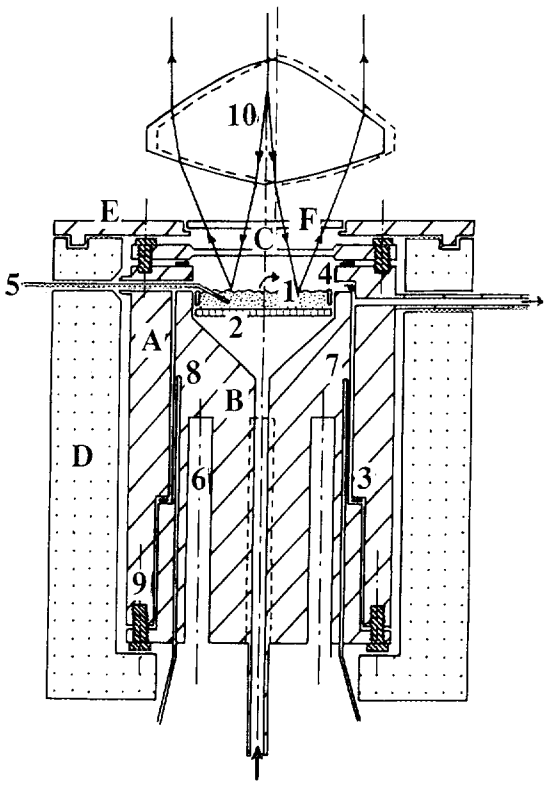

FIG. 1. Scheme of the *in situ* Raman cell (8, 23). (A) Chamber upper part; (B) chamber lower part; (C) glass window; (D) isolating shell: (E) thermal screen; (F) anticaloric filter. (1) Catalyst; (2) sintered glass; (3, 4) tightening rings; (5) temperature controller; (6) heating finger lodging; (7) chamber heating controller, (8) thermal security; (9) mounting bolts; (10) rotating lens.

heated at 120°C in order to avoid any condensation of the reaction products. Helium was the carrier gas (8).

Raman spectra were recorded on a Dilor Omars 89 spectrophotometer equipped with an intensified photodiode array detector. The emission line at 514.5 nm from Ar^+ ion laser (Spectra Physics Model 164) was used for excitation. The power of the incident beam on the sample was 30 mW. The time of acquisition was adjusted according to the intensity of the Raman scattering. To improve the signal-to-noise ratio, 100 spectra were accumulated for each spectrum. The wavenumber values obtained from the spectra were accurate to within about 2 cm^{-1}. To reduce both thermal and photodegradation of samples, the laser beam was scanned on the sample surface by means of a rotating lens. The scattered light was collected in the backscattering geometry.

The three precursors and the VPO catalysts after examination by *in situ* laser Raman spectroscopy were characterized by XRD diffraction using a Siemens diffractometer using Cu$K\alpha$ radiation and by electron microscopy techniques (TEM and STEM) using a JEOL JEM 2010 microscope to study the dispersion of the VPO phases and of the two doping Co and Fe elements. Atomic level dispersion of Co and Fe was evidenced by STEM for the two doped precursors (23).

The final catalysts were examined also by UV-visible, ^{31}P NMR by spin-echo mapping, electrical conductivity and XPS. UV-visible spectra were recorded on a Perkin–Elmer lambda 9 spectrometer equipped with an integration sphere.

^{31}P NMR spin-echo spectra were recorded on a Bruker MSL 300 NMR spectrometer, under static conditions, using a $90°x$-τ-$180°y$-τ-acquire sequence. The 90° pulse was 4.2 μs and τ was 20 μs. For each sample, the irradiation frequency was varied in increments of 100 kHz above and below the ^{31}P resonance of H_3PO_4. The number of spectra thus recorded was dictated by the frequency limits beyond which no spectral intensity was visible. The ^{31}P NMR spin-echo mapping information was then obtained by superposition of all spectra.

The semiconductivity of the different VPO samples after *in situ* Raman has been investigated by using a cell especially designed to study the electronic interactions between powdered samples and various gaseous atmospheres (24). This cell has already been employed for studying reference VPO phases (10). About 250 mg of the powder are deposited between two platinum electrodes under a constant pressure of ca. 10^5 Pa, which is compatible with good interparticular electrical contacts and with a good gas–solid interaction over the whole surface of the solid. Measurements have been performed at room temperature after degazing under vacuum (10^{-2} Torr). The electrical resistance of the samples has been measured with a Kontron multimeter (Model DMM 4021). Since, in this work, all the VPO samples had BET surface areas of the same order of magnitude, semiquantitative comparisons between VPO solids have been made to examine the influence of doping by Co and Fe.

XPS examinations of the VPO materials were performed with an Escalab 200 R machine using the Al$K\alpha$ radiation. The binding energy of adventitious carbon was taken as reference at 284.5 eV. Examination was directed toward binding energies of P_{2_p}, C_{1_s}, $V_{2_p}^{3/2}$ (V^{5+} and V^{4+}), $Co_{2_p}^{3/2}$, $Fe_{2_p}^{3/2}$, and O_{1_s}.

RESULTS

Analysis of the Undoped and Doped Precursors

Chemical analysis shows that the Co and Fe are present in the two $VOHPO_4, 0.5\ H_2O$ structures with the expected Co/V (5.02%) and Fe/V (5.14%) atomic ratios. Figure 2 shows the XRD spectra of the doped precursors as referred to the undoped precursor. Only the characteristic lines of $VOHPO_4, 0.5\ H_2O$ are observed (19). The relative (001)/(220) intensities are modified with doping, particularly for

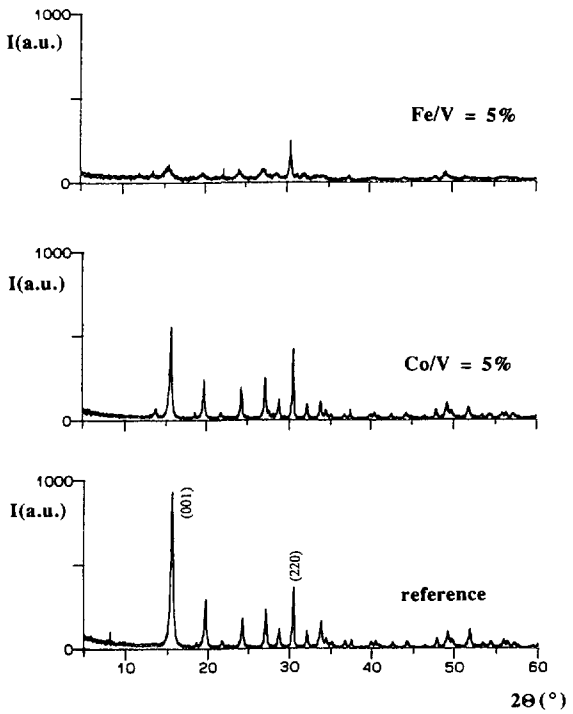

FIG. 2. XRD spectra of the three precursors.

Fe. This was confirmed from the STEM examination. The promoter appears to influence the morphology of the crystallites of the precursor. A STEM examination of the two doped precursors shows a good dispersion into the structure of the grains for the Fe promotor (mean value 4.7%), but a poorer one for the Co promoter (mean value 2.1%) (23).

Study of the Activation of the Undoped and Doped $VOHPO_4$, 0.5 H_2O as Studied by in Situ Raman Spectroscopy

Figure 3 presents the Raman spectra of the VPO reference phases: (i) $VOHPO_4$, 0.5 H_2O (V^{4+}) at room temperature prepared in aqueous medium under conditions previously described (8) and (ii) α_I-, α_{II}-, γ-, and δ-$VOPO_4$ (V^{5+}) and $(VO)_2P_2O_7$)(V^{4+}) under the *n*-butane/air atmosphere under reacting conditions.

Figure 3 shows that it is possible to study the activation of the $VOHPO_4$, 0.5 H_2O precursor to the $VOPO_4$ and $(VO)_2P_2O_7$ phases from the detection of their characteristic Raman bands. This has been previously evidenced for the precursor prepared in aqueous medium (8). It was observed that, with the increase of the temperature under the *n*-butane/air mixture, the structure of the vanadyl hemihydrate is progressively destroyed. Maleic anhydride appears in the stream as soon as both the $VOPO_4$ and $(VO)_2P_2O_7$ structures are detected by Raman. This seemed to demonstrate the necessity of the simultaneous presence of V^{4+} and V^{5+} sites on the VPO matrix to obtain maleic anhydride from *n*-butane oxidation.

Figure 4 and 5 show the evolution of the Raman spectra of the undoped $VOHPO_4$, 0.5 H_2O precursor, prepared according to the organic route, when temperature is increased under the *n*-butane/air mixture up to 430°C (ΔT = 1.25°C min^{-1}) (Fig. 4) and then maintained at this final temperature for a long period (Fig. 5). The decomposition of the precursor appears (Fig. 4) from the decrease of the band at 984 cm^{-1}. At variance with former experiments with the aqueous precursor (8), Raman spectra are of poor quality. The 984 cm^{-1} band only emerges from the fluorescence generated by residual isobutanol molecules trapped into the structure of the material (a pretreatment of this precursor under nitrogen at 250°C improved the intensity of the spectrum by desorption of isobutanol). At 370–400°C, the structure of the VPO material appears totally amorphous while, at the same temperature, the presence of $VOPO_4$ structures was detected on the VPO material generated from the aqueous precursor (8). As

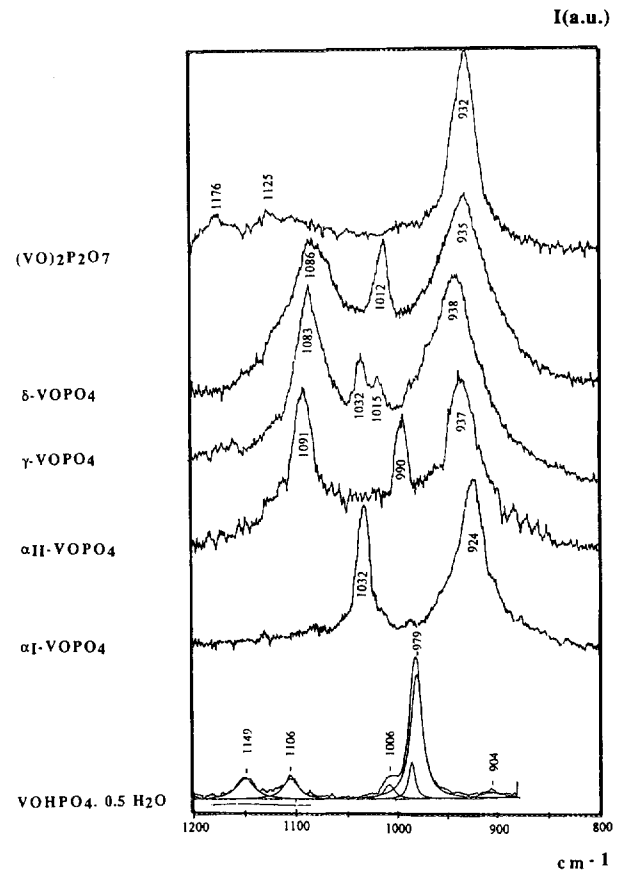

FIG. 3. Raman spectra of the VPO reference phases. Spectrum for $VOHPO_4 \cdot 0.5H_2O$ corresponds to the precursor prepared according to the aqueous route (8).

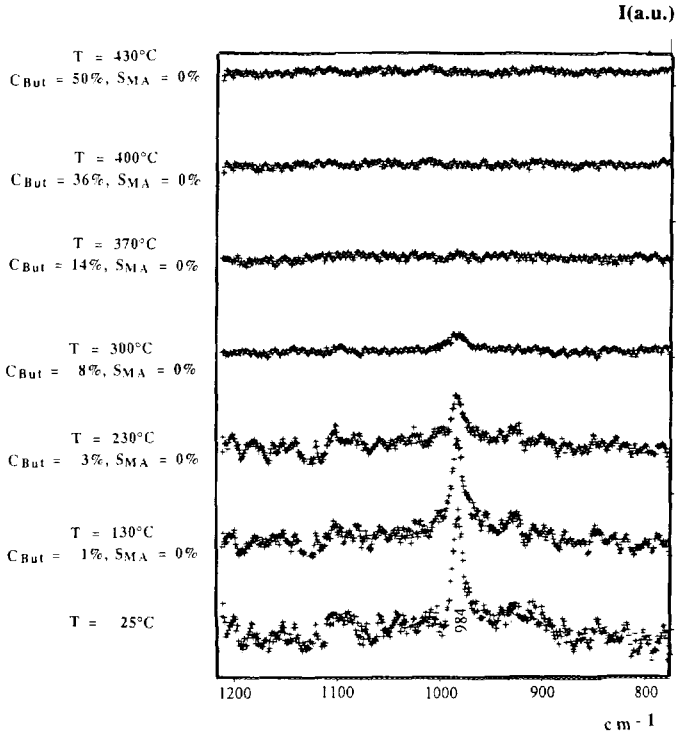

FIG. 4. Raman spectra obtained by treatment of the undoped $VOHPO_4 \cdot 0.5H_2O$ precursor from 25 up to 430°C under catalytic mixture (ΔT = 1.25°C min^{-1}).

soon as (t = 16 h, 15 min) the characteristic bands of $(VO)_2P_2O_7$ at 932 cm^{-1} is observed (with minor bands at 1125 and 1176 cm^{-1}), maleic anhydride (MA) is detected, which did not occur during the first hours of heating. A broadband with low intensity is then detected in the 1070–1140 cm^{-1} range for longer times (35 h, 45 min–66 h, 15 min), which is indicative of some $VOPO_4$ structure.

Figures 6 and 7 show the evolution of the Raman spectra in the case of the Co-doped precursor, under conditions previously described. It is noticeable that, when increasing the temperature (Fig. 6), an intense $VOPO_4$ signal at 1091 cm^{-1} appears while the $VOHPO_4, 0.5\ H_2O$ structure (signal at 984 cm^{-1}) is not yet decomposed. This corresponds to the simultaneous detection of MA in the stream. Catalytic performances improve rapidly up to 430°C where $(VO)_2P_2O_7$ is detected (signals at 932 and 1176 cm^{-1}) as well as $VOPO_4$ (signal at 1090 cm^{-1}). The corresponding 1090 cm^{-1} shoulder is intense, which should correspond to a higher $VOPO_4$ content with a better dispersion as compared to the same situation for the undoped VPO catalyst (Fig. 3). The evolution of the Raman spectra with time at 430°C (Fig. 7) confirms the importance of the simultaneous presence of $VOPO_4$ and $(VO)_2P_2O_7$ structure for improving selectivity to MA, but it is noticeable that MA was observed in the feed stream with the detection of the $VOPO_4$ structures and prior to the detection of $(VO)_2P_2O_7 \cdot \alpha_{II}$-$VOPO_4$ is detected (signal at 990 cm^{-1}) after 63 h. The comparison of Figs. 7 and 5 shows a higher $VOPO_4/(VO)_2P_2O_7$ ratio for the Co-doped VPO catalyst as compared to the undoped one (compare the relative ratio of the 1090 cm^{-1}/932 cm^{-1} bands). Selectivity to MA is also much higher for comparable n-butane conversion for the Co-doped VPO catalyst.

Figures 8 and 9 show the evolution of the Raman spectra for the temperature increase up to 430°C (ΔT = 1.25°C min^{-1}) (Fig. 8) and at 430°C (Fig. 9) in the case of the Fe-doped precursor, under conditions previously described. Comparison of Figs. 8 and 6 shows that as for the Co-doped precursor, the detection of MA in the stream for the Fe-doped precursor is observed when the signal at 1091 cm^{-1} associated to $VOPO_4$ appears on the Raman spectrum at 250°C. It corresponds also to a situation in which the hemihydrate is not yet decomposed. Signals at 932 and 1176 cm^{-1} associated to $(VO)_2P_2O_7$ appear at lower temperature, which is not associated to a higher MA selectivity. Comparison of catalytic performances on the two doped catalysts shows that for similar n-butane conversion, selectivity to MA is lower for the Fe-doped catalyst with respect to the Co-doped one. This should be due to

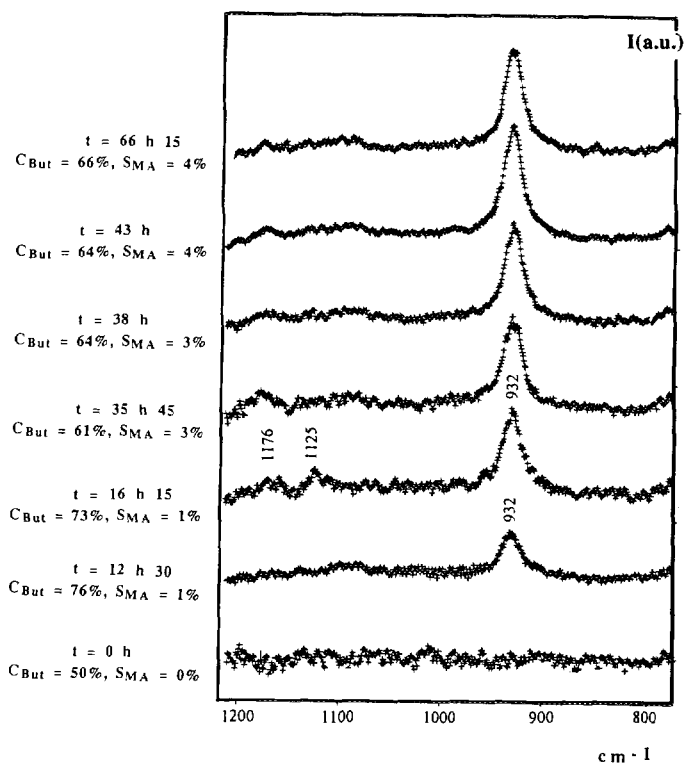

FIG. 5. Raman spectra at 430°C of the VPO catalyst obtained by treatment of the undoped $VOHPO_4 \cdot 0.5H_2O$ precursor under catalytic mixture.

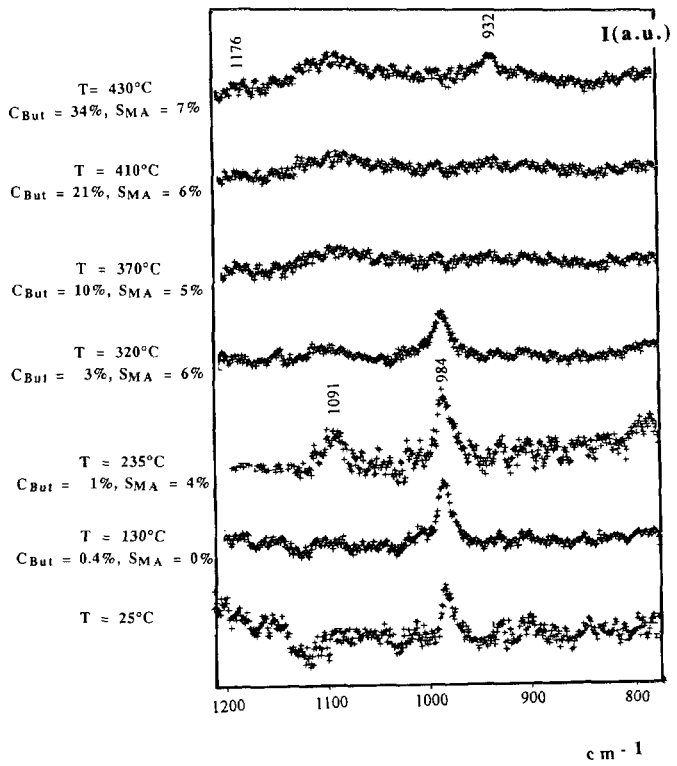

FIG. 6. Raman spectra obtained by treatment of the Co-doped $VOHPO_4 \cdot 0.5H_2O$ precursor from 25 up to 430°C under catalytic mixture (ΔT = 1.25°C min^{-1}).

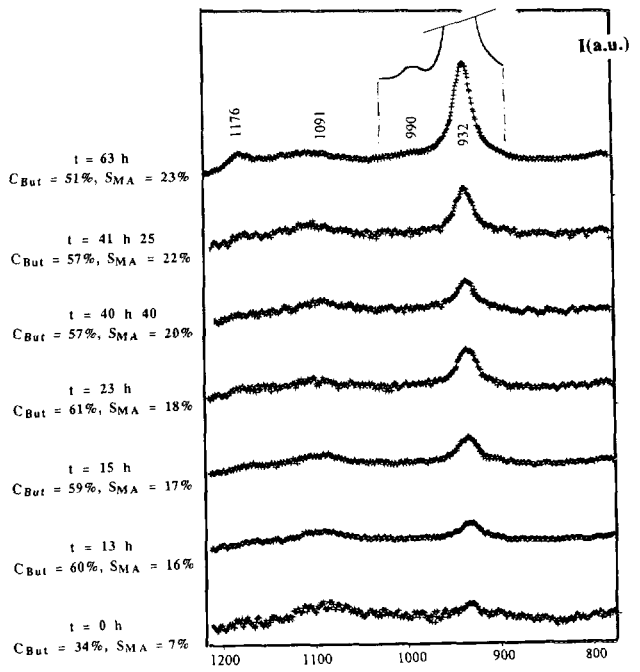

FIG. 7. Raman spectra at 430°C of the VPO catalyst obtained by treatment of the Co-doped $VOHPO_4 \cdot 0.5H_2O$ precursor under catalytic mixture.

a different $VOPO_4/(VO)_2P_2O_7$ ratio with different dispersion of these two phases.

It is also important to note that all the Raman spectra can be indexed only as VPO phases (22). No new bands appear in the 800–1200 cm^{-1} range, which should be assigned to any Co or Fe phosphate. This favors a good dispersion of the two dopants into the VPO structures as observed by STEM in their corresponding precursors (23).

Study of the Physicochemistry of Undoped and Doped VPO Catalysts after in Situ Raman Examination

XRD spectra of the three catalysts are shown in Fig. 10 in the 10–60°2Θ range. They are characteristic of $(VO)_2P_2O_7$ only. The different relative intensities of the main lines is indicative of different morphologies of the corresponding crystallites, which was evidenced by SEM (23).

UV-visible spectra of the catalysts is presented in Fig. 11 with the spectrum of pure $(VO)_2P_2O_7$. A high-intensity charge-transfer band is observed at 280 nm. The two bands at 880–900 and 660 nm correspond to the same V^{4+} species in octahedral symmetry (25). V^{5+} species in an octahedral environment are evidenced by the small band at 500 nm

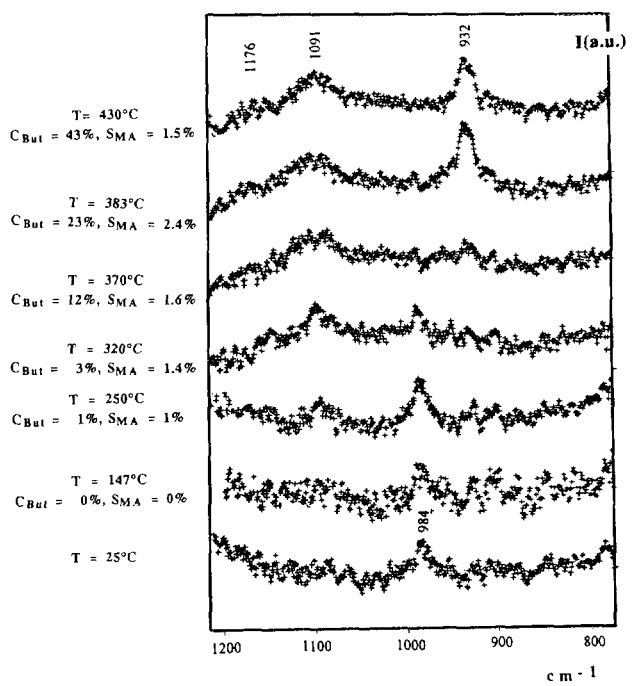

FIG. 8. Raman spectra obtained by treatment of the Fe-doped $VOHPO_4 \cdot 0.5H_2O$ precursor from 25 up to 430°C under catalytic mixture (ΔT = 1.25°C min^{-1}).

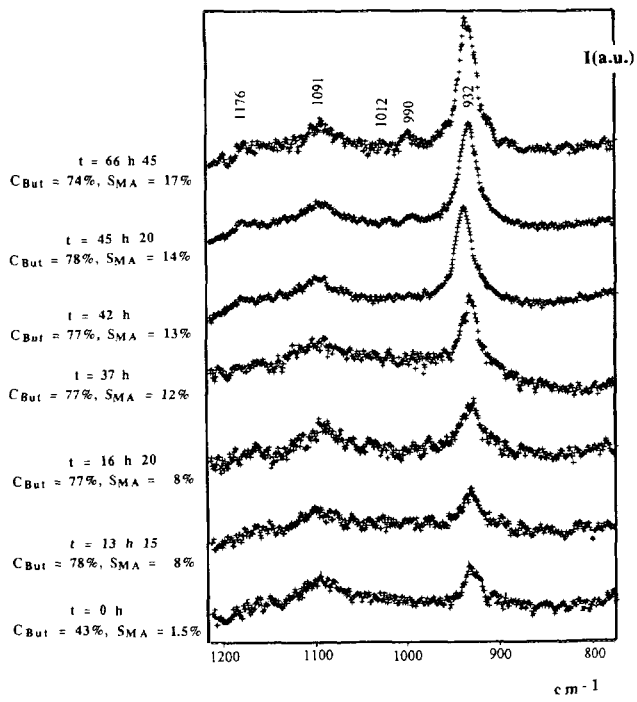

FIG. 9. Raman spectra at 430°C of the VPO catalyst obtained by treatment of the Fe-doped $VOHPO_4 \cdot 0.5H_2O$ precursor under catalytic mixture.

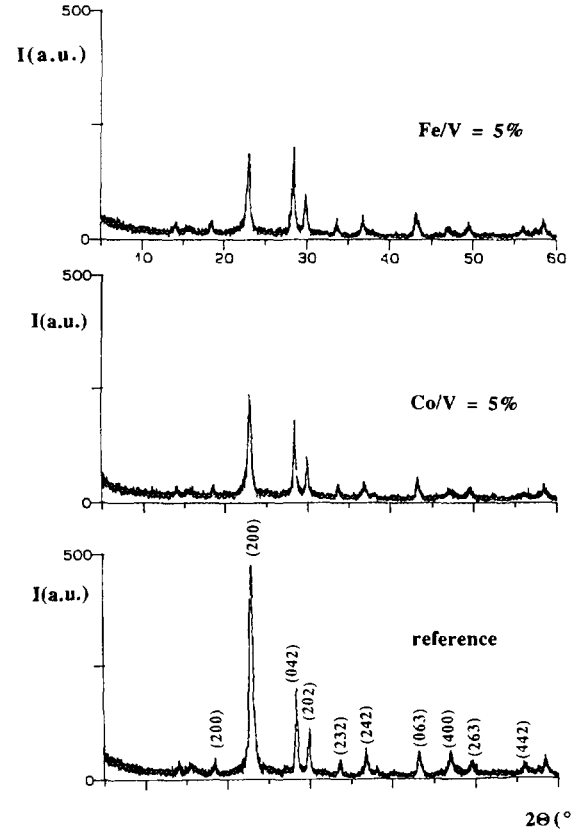

FIG. 10. XRD spectra of the three catalysts after *in situ* Raman examination.

(26). The higher $VOPO_4$ (V^{5+})/$(VO)_2P_2O_7$ (V^{4+}) ratio for the doped VPO catalysts as referred to the undoped VPO catalyst is evidenced from the higher ratio for the relative intensities between the 500-nm and the two 660- and 900-nm bands. This is in agreement with the examination by Raman.

Figure 12 shows the ^{31}P NMR by spin-echo mapping of the three catalysts. Signal at approximately 2600 ppm is attributed to P atoms connected to V^{4+} in the structure of $(VO)_2P_2O_7$, while signal near 0 ppm corresponds to P atoms connected to V^{5+} sites (27). It is obvious, as observed by the other techniques, that doping by Co and Fe increases strongly the ratio $VOPO_4/(VO)_2P_2O_7$. No signal is observed at 4650 ppm, which should be indicative of P atoms connected to V^{3+} sites.

XPS measurements are summarized in Table 1. $V_{2p^{3/2}}$ peaks of the three catalysts are relatively large (2.3–2.4 eV). Previous studies have shown that binding energies for V^{4+} and V^{5+} are separated by 1 eV (28, 29). Therefore we have considered that the $V_{2p^{3/2}}$ peak is the contribution of the two oxidations V^{4+} and V^{5+}. Taking into account previous conditions of decomposition of these two peaks (9), we have calculated the V^{4+} and V^{5+} percentage in the three catalysts. It is shown in Table 1 that Co induces an increase of the V^{5+}/V contribution, which is not observed in the case of doping by Fe. Another interesting result is the observation of a surface P enrichment for both doped VPO catalysts.

Electrical conductivity measurements have been performed at room temperature (to avoid any oxidation) on the VPO catalysts and referred to pure $(VO)_2P_2O_7$. Figure 13 shows the logarithm transform of the electrical conductivity σ as a function of time on degassing for the pure $(VO)_2P_2O_7$ phase and for the undoped VPO catalyst. The decrease of conductivity has been explained by a slow dehydroxylation of the surface of the solids (10). In stationary conditions, a higher conductivity (by a factor of 2.5) is observed for the VPO catalyst as compared to the pure $(VO)_2P_2O_7$ phase. Figure 14 shows the difference for the conductivity under similar experimental conditions between the two doped VPO catalysts and the undoped one. Under stationary conditions the Co- and Fe-doped VPO are more conductive. These two results are discussed in the next section.

DISCUSSION

The XRD examination of the two doped precursors shows the only presence of the $VOHPO_4$, 0.5 H_2O struc-

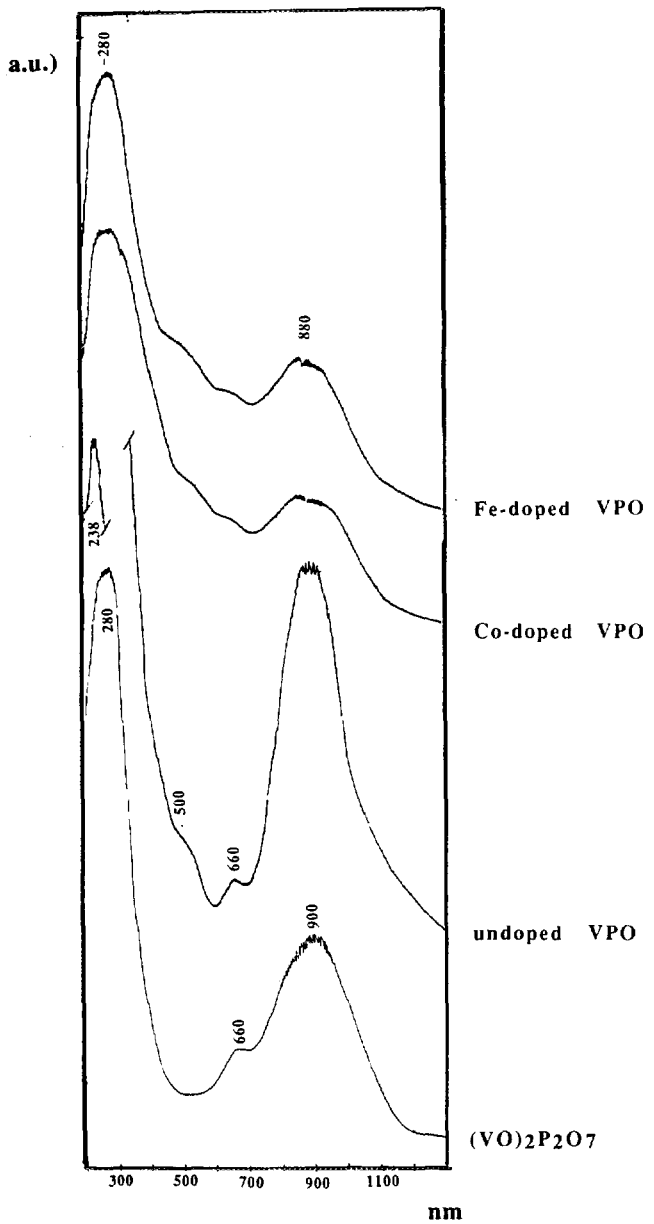

FIG. 11. UV-visible spectra of the VPO catalysts after *in situ* Raman referred to $(VO)_2P_2O_7$. $(VO)_2P_2O_7$ was prepared by calcination of $VOHPO_4 \cdot 0.5H_2O$ under nitrogen at 860°C.

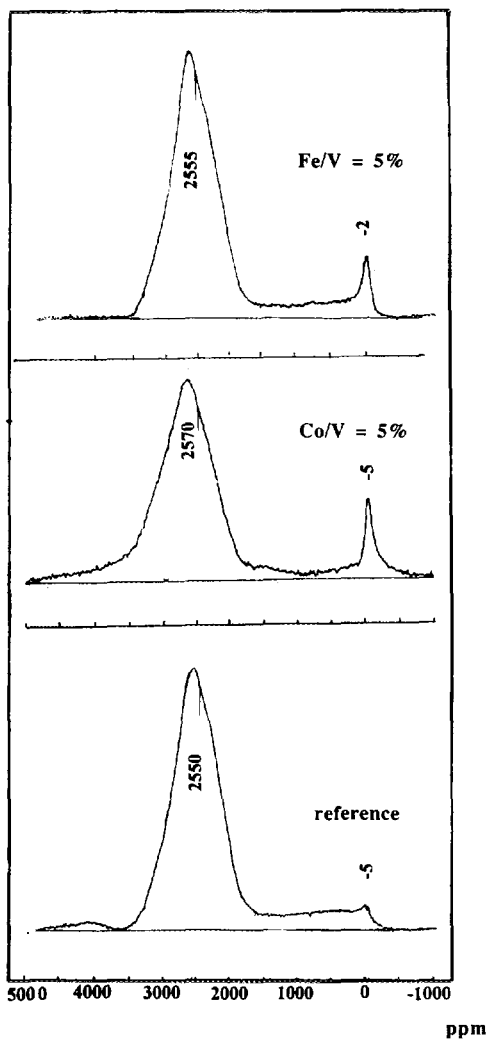

FIG. 12. ^{31}P spin-echo mapping of the VPO catalysts after *in situ* Raman.

ture while STEM examination shows a good dispersion for Fe and a poorer dispersion for Co (23). No other structures are detected. It can thus be considered that Fe is better dispersed into the $VOHPO_4$, 0.5 H_2O structure than Co.

The Raman spectra obtained from the three $VOHPO_4$, 0.5 H_2O precursors prepared according to the organic route present a poor intensity as compared to the spectra obtained from the undoped precursor prepared by the aqueous route (8). This was explained by fluorescence gener-

TABLE 1

XPS Results on the Three Catalysts after *in Situ* Raman Examination

Catalysts	Undoped VPO	Co-doped VPO	Fe-doped VPO
Be[a] P_{2p}(eV)	131.7	131.7	131.7
BE $V^{5+}2p$(eV)	518.0	518.0	517.8
BE $V^{4+}2p$(eV)	516.9	516.9	516.7
BE O_{1s}(eV)	730.5	730.5	730.5
P/V (%)	1.84	2.10	2.06
Co/V (%)	—	12.6	—
Fe/V (%)	—	—	6.4
V^{5+}/V (%)	17.5	23.0	12.0
V^{4+}/V (%)	82.5	77.0	88.0
V^{5+}/V^{4+} (%)	21.2	30.0	13.6

[a] Binding energies (eV).

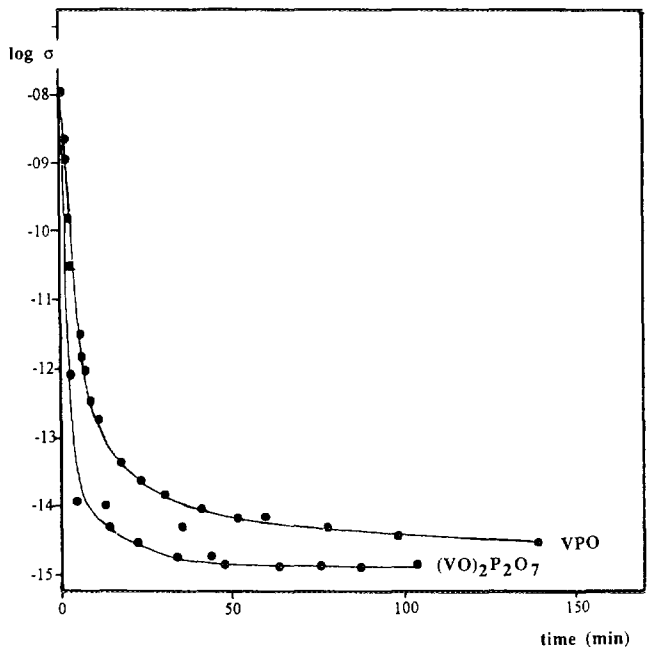

FIG. 13. Semilogarithmic transform of the electrical conductivity (σ) as function of time for the undoped VPO catalyst after *in situ* Raman as referred to $(VO)_2P_2O_7$.

ated by the isobutanol molecules intercalated into the lamellar structure of the materials. The 984 cm^{-1} band was the only significant feature in these spectra (Figs. 4, 6, and 8; T = 25°C).

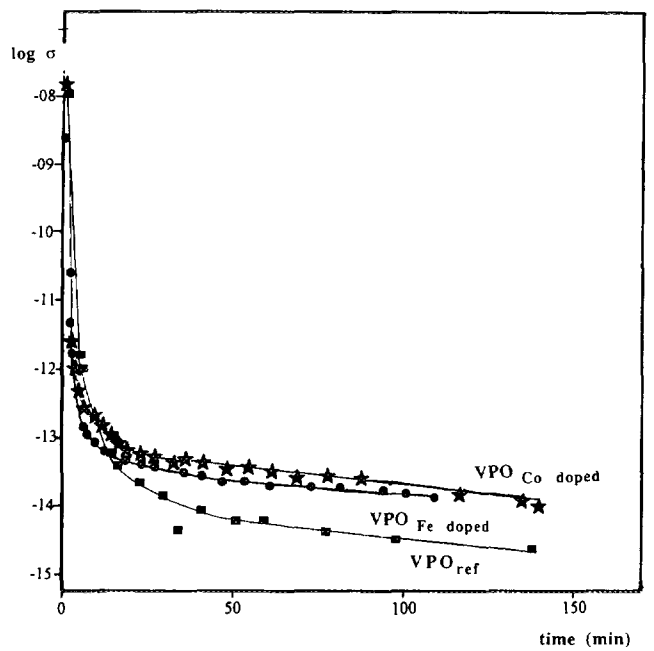

FIG. 14. Semilogarithmic transform of the electrical conductivity (σ) as function of time for the two doped VPO catalysts after *in situ* Raman as referred to the undoped catalyst.

The decomposition of the undoped organic precursor by increasing temperature under the *n*-butane/air reacting mixture goes through an amorphous phase as observed in the case of the aqueous precursor (8). MA is observed at the moment where Raman signals associated to $(VO)_2P_2O_7$ and $VOPO_4$ phases are detected. This is in agreement with our previous observations (8). However in the case of the organic precursor, the activation appears to require longer time than the aqueous precursor. This delay can be explained by the difficulty to desorb isobutanol from the VPO material in the first case. For the undoped VPO catalyst, $VOPO_4$ phases are difficult to detect due to their low amount and poor crystallinity as compared to $(VO)_2P_2O_7$. Nevertheless, their presence, impossible to evidence by XRD, was confirmed by the examination of the Raman spectra registered at lower temperature (380°C) under catalytic conditions and after cooling at room temperature by UV-visible spectroscopy and by ^{31}P NMR by spin-echo mapping.

Doping by Co or Fe strongly influences the physicochemical transformation of the $VOHPO_4$, 0.5 H_2O precursor. It is noticeable that the $VOPO_4$ structures appear while the decomposition of the hemihydrate is not achieved and prior to the detection of any $(VO)_2P_2O_7$ signal. This is simultaneously associated with the presence of MA in the gas stream. In this case, MA can be produced on a V^{5+}/V^{4+} matrix where V^{4+} comes from the $VOHPO_4$, 0.5 H_2O precursor. Fe appears to delay, more than Co, the decomposition of the hemihydrate structure.

The comparison of the Raman spectra and the catalytic performances at the end of the period at 430°C confirms the beneficial role of the $VOPO_4$ structures on $(VO)_2P_2O_7$ (V^{5+}/V^{4+} matrix, where, in this case, V^{4+} comes from the $(VO)_2P_2O_7$ pyrophosphate): doping by Co and Fe strongly enhances the contribution of the $VOPO_4$ phases. These phases appear to be much more dispersed in the case of doping by Co: Raman characteristic lines near 1090 cm^{-1} are very large. It is difficult to discriminate between α_{II}-, γ-, and δ-$VOPO_4$ in this case when α_{II}- and/or γ-, δ- $VOPO_4$ are easily evidenced in the case of doping by Fe with Raman characteristic lines at 990 and 1012 cm^{-1}, respectively. In a recent publication (9), it has been demonstrated that the activation of the hemihydrate goes first through a surface oxidation of the VPO catalyst grains to $VOPO_4$ (oxidation period), which is followed by a progressive reduction of their surface to $(VO)_2P_2O_7$ (reduction period).

Figure 15 shows the evolution of the catalytic performance in the Raman cell with the time on activation at 430°C. The variation of *n*-butane conversion and MA selectivity visualize this evolution and explain the effect of the two promoters. The oxidation period corresponds, for the three catalysts, to the first 10 h where *n*-butane conversion increases simultaneously with the increase of the superficial V^{5+}/V^{4+} ratio. During this period, the VPO catalysts have

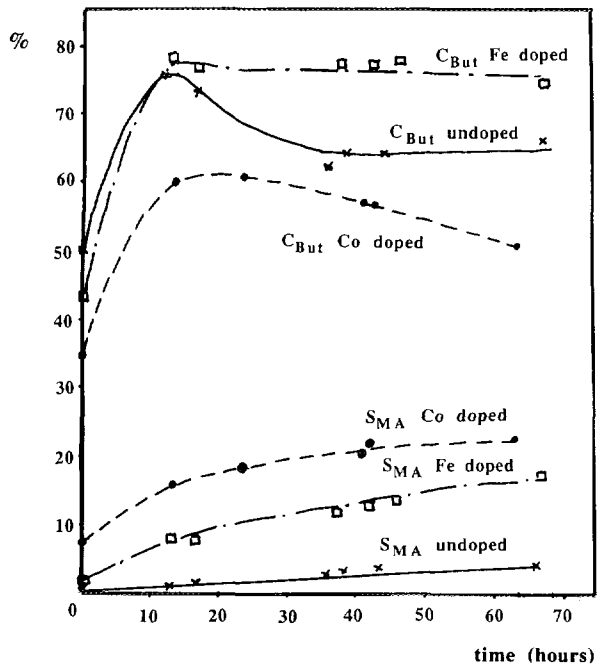

FIG. 15. Variation of the catalytic performances in the *in situ* raman cell under the reacting *n*-butane/air mixture at 430°C as function of time. (x) *n*-C4 conversion for undoped VPO catalysts; (●) *n*-C4 conversion for Co-doped VPO catalyst; (□) *n*-C4 conversion for Fe-doped VPO catalyst. (x) S_{MA} for undoped VPO catalyst, (●) S_{MA} for Co-doped VPO catalyst; (□) S_{MA} for Fe-doped VPO catalyst.

a poor crystallinity. The difference in the role of the two promoters appears after 10 h during the reduction period where the superficial V^{5+}/V^{4+} ratio decreases: *n*-butane conversion is stabilized when doping by Fe while it decreases for the undoped and Co-doped catalysts. This can be explained by the fact that Fe has been observed to be much better dispersed than Co in the original $VOHPO_4$, 0.5 H_2O matrix (23) and also by the fact that the redox potential Fe^{3+}/Fe^{2+} (0.75 V/NHE) is lower than the redox potential V^{5+}/V^{4+} (1V/NHE) in comparison with that of Co^{3+}/Co^{2+} (1.85 V/NHE). Fe introduced as Fe^{3+} in the $VOHPO_4$, 0.5 H_2O precursor is not able to displace V^{4+} to V^{5+}, which is the case for Co^{3+}. During the reduction period, the crystallinity of the VPO catalyst improves. Note that MA selectivity improves continuously during all this time of activation.

Depending on its redox potential and on its dispersion, the role of the promoter is to control the V^{5+}/V^{4+} balance during the activation period of the VPO catalyst, and this will influence continuously the *n*-butane conversion and the MA selectivity. Thus, the $VOPO_4/(VO)_2P_2O_7$ surface distribution on the catalyst grains and the crystallinity of this V^{4+}–V^{5+} matrix will be the key factor. After the experiments in the *in situ* Raman cell, the Fe-doped VPO catalyst presented a BET area (26 $m^2\ g^{-1}$) almost similar to that of the undoped VPO catalyst (27 $m^2\ g^{-1}$), while that of the Co doped was slightly lower (21 $m^2\ g^{-1}$) (Table 2). Intrinsic activities measured for the two doped VPO catalysts confirmed a strong increase as compared to the undoped VPO one, but lower than that observed for VPO laboratory samples (Table 2) (30).

The different physicochemical tools used to examine the VPO catalysts after the *in situ* Raman activation give us information on the bulk (XRD, UV visible, ^{31}P spin-echo mapping, and electrical conductivity) and on the surface (XPS) composition when the three catalysts have been cooled at room temperature.

XRD detects only $(VO)_2P_2O_7$ on the three final catalysts while UV visible and ^{31}P spin-echo mapping detect also the presence of $VOPO_4$ phases with a high increase of this amount for the two doped catalysts. The two dopants have an influence on the morphology of the $(VO)_2P_2O_7$ crystallites, as evidenced by SEM (23).

The electrical measurements give us information on the eventual modifications induced to the V^{4+} matrix of $(VO)_2P_2O_7$ by V^{5+} and by Co^{3+} and Fe^{3+} doping ions. The undoped VPO catalyst presents a higher conductivity as compared to pure $(VO)_2P_2O_7$, which can be interpreted by a dissolution of V^{5+} into the $(VO)_2P_2O_7$ matrix. Doping by Co and Fe increases the conductivity of the final catalysts by a factor 4.5 as compared to the undoped one. According to the induction valence law (31), this can be interpreted only by the substitution of VO^{2+} vanadyl cations of the $(VO)_2P_2O_7$ matrix by Co^{3+} and Fe^{3+}. As the values of conductivity under stationary conditions are al-

TABLE 2

Comparison of the Intrinsic Activities I.A. Measured for the Three VPO Catalysts for *n*-Butane Oxidation at 430°C and after 63–66 h in the *in Situ* Raman Cell as Compared to Results Previously Published on Laboratory Samples (30)

Catalysts	S_{BET} ($m^2\ g^{-1}$)	C_{But} (%)	S_{MA} (%)	Y_{MA} (%)	I.A.[c] × 10^5 (mol MA $m^{-2}\ h^{-1}$)
Undoped VPO[a]	27	66	4	2.6	0.17
Co-doped VPO[a]	21	51	23	11.7	1.00
Fe-doped VPO[a]	26	74	17	12.6	0.86
VP(A)[b]	4	11	51	5.6	1.24
VP(O)[b]	14	27	52	14.0	1.35

[a] Present *in situ* Raman cell study: 430°C, 63–66 h. But/air, 1.5%; GSHV, 2000 h^{-1}; ρ_{cat}, 1.33.

[b] Results published in Ref. (30): 390°C, 72 h. But/air, 1.5%; GSHV, 1000 h^{-1}; ρ_{cat}, 1.00.

[c] Calculated using the corresponding formula:

$$\text{I.A. (mol MA m}^{-2}\text{ h}^{-1}) = \frac{\%\ \text{But/air} \times \text{GSHV (h}^{-1}) \times \rho_{cat}\ (\text{ml g}^{-1}) \times Y_{MA}\ (\%)}{22400\ (\text{ml mol}^{-1}) \times S_{BET}\ (\text{m}^2\ \text{g}^{-1})}.$$

most the same, this shows a similar behavior of the two promotors on the bulk properties of $(VO)_2P_2O_7$.

Finally the examination of the XPS results (Table 1) give us interesting informations on the V^{5+}/V^{4+} superficial ratios after the *in situ* activation at 430°C in the Raman cell. Doping VPO by Co^{3+} has strongly enhanced the V^{5+}/V^{4+} ratio at the surface due to the favorable Co^{3+}/Co^{2+} potential redox value, while doping VPO by Fe^{3+} decreases this ratio. The increase of the superficial P/V ratio with doping by Co^{3+} and Fe^{3+} confirms similar observations made by other authors in the case of Co (14). It is also logical to observe a high superficial amount of Co (Co/V = 12.6%) since it was observed by STEM that the dispersion of Co was poor in the starting Co-doped $VOHPO_4$, 0.5 H_2O precursor (Co/V = 2.1% instead of 5%) as compared to the dispersion of Fe in the starting Fe-doped $VOHPO_4$, 0.5 H_2O precursor (Fe/V = 4.7% instead of 5%). By XPS the superficial amount is Fe/V = 6.4%, which is very near the 5% bulk composition. This confirms the fact that there was no Fe segregation during the activation period in the Raman cell.

ACKNOWLEDGMENTS

The authors are indebted to Dr. J. M. Herrmann for discussion and assistance in the electrical conductivity measurements, to C. Leclercq for the electron microscopy examinations, to M. Brun for the XPS examinations, and to Dr. A. Tuel and Dr. G. Coudurier for discussion of the ^{31}P NMR by spin-echo mapping and UV-visible results, respectively.

REFERENCES

1. Varma, R. A., and Saraf, D. N., *Ind. Eng. Chem. Prod. Res. Dev.* **18,** 7 (1979).
2. Hodnett, B. K., Permanne, Ph., and Delmon, B., *Appl. Catal.* **6,** 231, (1983).
3. Hodnett, B. K., *Catal. Rev.-Sci. Eng.* **27,** 373 (1985).
4. Centi, G., Trifiro, F., Ebner, J. R., and Franchetti, V. M., *Chem. Rev.* **88,** 55 (1988).
5. G. Centi, Ed., "Vanadyl Pyrophosphate Catalysts," Vol. 16, No. 1. Elsevier, Amsterdam, 1993.
6. Hodnett, B. K., *Catal. Today* **1,** 477 (1987).
7. Zhang, Y. Sneeden, R. P. A., and Volta, J. C., *Catal. Today* **16,** 39 (1993).
8. Hutchings, G. J., Desmartin-Chomel, A., Olier, R., and Volta, J. C., *Nature* **368,** 41 (1994).
9. Abon, M., Bere, K. E., Tuel, A., and Delichere, P., *J. Catal.*, in press.
10. Rouvet, F., Herrmann, J. M., and Volta, J. C., *J. Chem. Soc., Faraday Trans.* **90,** 1441 (1994).
11. Hutchings, G. J., *Appl. Catal.* **72,** 1 (1991).
12. Hodnett, B. K., and Delmon, B., *Appl. Catal.* **6,** 245 (1983).
13. Zazhigalov, V. A., Haber, J., Stoch, J., Pyatnitzkaya, A. I., Komashko, G. A., and Belousov, V. M., *Appl. Catal. A: General* **96,** 135 (1993).
14. Takita, Y., Tanaka, K., Ichimaru, S., Mizihara, Y., Abe, Y., and Ishihara, T., *Appl., Catal. A: General* **103,** 281 (1993).
15. Brutovsky, M., and Gerej, S., *Czech. Chem. Commun.* **47,** 403 (1982).
16. Brutovsky, M., Gerej, F., Vasilco, F., and Gerejova, J., *Czech. Chem. Commun.* **47,** 1290 (1982).
17. Otake, M., U.S. Patent 4 337 173 (1982), assigned to Mitsubishi Chem. Ind.
18. Li, J., Lashier, M. E., Schrader, G. L., and Gerstein, B. C., *Appl. Catal.* **74,** 15 (1994).
19. Johnson, J. W., Johnston, D. C., Jacobson, A. J., and Brody, J. F., *J. Am. Chem. Soc.* **106,** 8123 (1984).
20. Ellison, I. J., Hutchings, G. J., Sananés, M. T., and Volta, J. C., *J. Chem. Soc. Chem. Commun.*, 1093 (1994).
21. Hutchings, G. J., Olier, R., Sananés, M. T., and Volta, J. C., *in* "New Developments in Selective Oxidation" (V. Cortés Corberan and S. Vic Bellon, Eds.), Studies in Surface Sci., Vol. 82, p. 213. Elsevier, Amsterdam, 1994.
22. Ben Abdelouahab, F., Olier, R., Guilhaume, N. Lefebvre, F., and Volta, J. C., *J. Catal.* **134,** 151 (1992).
23. Ben Abdelouahab, F., Ziyad, M., Leclercq, C., Millet, J. M., Olier, R., and Volta, J. C., *J. Chim. Phys.* **92,** 1320 (1995).
24. Herrmann, J. M., *in* "Les Techniques Physiques d'Etude des Catalyseurs" (B. Imelik and J. C. Védrine, Eds.), p. 753. Technip, Paris, 1988.
25. Loukah M., Coudurier, G., Védrine, J. C., and Ziyad, M., *Microporous Mater.*, **4,** 345 (1995).
26. Schraml-Marth, M., Wokaun, A., and Baiker, A., *J. Catal.* **124,** 86 (1990).
27. Sananés, M. T., Tuel, A., and Volta, J. C., *J. Catal.* **145,** 251 (1994).
28. Garbassi, F., Bart, J. C., Tassinari, R., Vlaic, G., and Lagarde, P., *J. Catal.* **98,** 317 (1986).
29. Moser, T. P., and Schrader, G. L., *J. Catal.* **104,** 99 (1987).
30. Sananés, M. T., Hutchings, G. J., and Volta, J. C., *J. Catal.* **154,** 253 (1995).
31. Herrmann, J. M., *in* "Catalyst Characterization—Physical Techniques for Solid Materials" (B. Imelik and J. C. Védrine, Eds.), Chap. 20, p. 559. Technip, Paris, 1994.